3162 *Inorg. Chem.* **2010**, *49*, 3162–3168
DOI: 10.1021/ic901998p

Inorganic Chemistry
Article

Magnetic Bistability in a Cobalt Bis(dioxolene) Complex: Long-Lived Photoinduced Valence Tautomerism

Robert D. Schmidt, David A. Shultz,* and James D. Martin

Department of Chemistry, North Carolina State University, Raleigh, North Carolina 27695-8204

Received October 8, 2009

The thermal- and photoinduced valence tautomerism of a cobalt bis(dioxolene) complex is described. The thermal conversion is precipitous, complete within 10 K, and is accompanied by a 5 K hysteresis loop (107 K < $T_{1/2}$ < 112 K). Rapid thermal quenching (300 K → 10 K in ca. 5 s) and photoinduced valence tautomerism result in trapping of the metastable Co^{II}-state at low temperatures through intermolecular hydrogen bonding. This lattice stabilization results in unmatched kinetic and thermal stability for a valence tautomer from 10−50 K, with residual *hs*-Co^{II} persisting until about 90 K.

Introduction

There is a large area of research dedicated to iron-based spin crossover complexes, specifically those that demonstrate thermal hysteresis.[1−3] A more specialized effect, light-induced excited state spin trapping (LIESST),[1,2,4,5] has garnered a great deal of interest, because of the accessibility and stability of metastable states. These phenomena predominately rely on spin forbidden relaxation processes to provide the mechanism for metastability.[2,4,6] LIESST complexes are characterized by the accessibility of a metastable excited-state through irradiation with specific wavelengths of light below the decay temperature (T_{LIESST}), and some are accompanied by a thermal hysteresis loop above T_{LIESST} in the warming and cooling modes.[5,7−9] This metastable state is generally the high temperature stable form of the complex, which presents very long lifetimes and high thermal stability.[1,2,4−7,9,10] While the field of iron-based systems is vast, there is a paucity of examples utilizing other redox-active metal complexes, such as cobalt valence tautomers.

Molecules that demonstrate intramolecular electron transfer accompanied by a single-site spin crossover are termed "valence tautomers."[11,12] The quintessential valence tautomeric equilibrium is the *ls*-Co^{III}(SQ)(Cat)L ↔ *hs*-Co^{II}(SQ)(SQ)L system, where SQ is a substituted *o*-semiquinonate, Cat is a substituted *o*-catecholate, and L is usually a redox innocent diimine ligand.[12] Several complexes of this type are known to demonstrate valence reorganization in response to external stimuli, such as temperature and pressure.[12,13] In some cases, this conversion can be induced by irradiation of a Co^{III} charge transfer band to yield the Co^{II} form, which is metastable at temperatures sufficiently low enough to afford slow relaxation kinetics.[14−17] There exists only a handful of complexes reported that demonstrate this "photoinduced" valence tautomerism, presenting very small stability ranges (10−50 K), and decay begins as soon as the light stimulus is removed.[17−20] Moreover, those complexes shown to demonstrate this photoactivity lack a common structural feature that can be used as a molecular design element for systematically

*To whom correspondence should be addressed. E-mail: david_shultz@ncsu.edu.

(1) Decurtins, S.; Gütlich, P.; Köhler, C. P.; Spiering, H.; Hauser, A. *Chem. Phys. Lett.* **1984**, *105*(1), 1–4.
(2) Gütlich, P.; Hauser, A. *Coord. Chem. Rev.* **1990**, *97*, 1–22.
(3) Gaspar, A. B.; Ksenofontov, V.; Seredyuk, M.; Gütlich, P. *Coord. Chem. Rev.* **2005**, *249*(23), 2661–2676.
(4) Gütlich, P.; Garcia, Y.; Woike, T. *Coord. Chem. Rev.* **2001**, *219*−*221*, 839–879.
(5) Létard, J.-F.; Capes, L.; Chastanet, G.; Moliner, N.; Létard, S.; Real, J.-A.; Kahn, O. *Chem. Phys. Lett.* **1999**, *313*(1−2), 115–120.
(6) Hauser, A. *Chem. Phys. Lett.* **1986**, *124*(6), 543–548.
(7) Létard, J.-F.; Guionneau, P.; Rabardel, L.; Howard, J. A. K.; Goeta, A. E.; Chasseau, D.; Kahn, O. *Inorg. Chem.* **1998**, *37*(17), 4432–4441.
(8) Capes, L.; Létard, J.-F.; Kahn, O. *Chem.—Eur. J.* **2000**, *6*(12), 2246–2255.
(9) Mishra, V.; Mukherjee, R.; Linares, J.; Balde, C.; Desplanches, C.; Létard, J.-F.; Collet, E.; Toupet, L.; Castro, M.; Varret, F. *Inorg. Chem.* **2008**, *47*(17), 7577–7587.
(10) Li, D.; Clerac, R.; Roubeau, O.; Harte, E.; Mathoniere, C.; Le Bris, R.; Holmes, S. M. *J. Am. Chem. Soc.* **2007**, *130*(1), 252–258.
(11) Shultz, D. A. Valence Tautomerism in Dioxolene Complexes of Cobalt. In *Magnetism: Molecules to Materials II*; Miller, J. S., Drillon, M., Eds.; Wiley-VCH: New York, 2001; Vol. *2*, pp 281−306.
(12) Buchanan, R. M.; Pierpont, C. G. *J. Am. Chem. Soc.* **1980**, *102*(15), 4951–4957.
(13) Adams, D. M.; Dei, A.; Rheingold, A. L.; Hendrickson, D. N. *J. Am. Chem. Soc.* **1993**, *115*(18), 8221–8229.
(14) Sato, O.; Hayami, S.; Gu, Z.-z.; Takahashi, K.; Nakajima, R.; Fujishima, A. *Phase Transitions* **2002**, *75*(7), 779–785.
(15) Cui, A.; Takahashi, K.; Fujishima, A.; Sato, O. *J. Photochem. Photobiol. A* **2004**, *167*(2−3), 69–73.
(16) Tao, J.; Maruyama, H.; Sato, O. *J. Am. Chem. Soc.* **2006**, *128*(6), 1790–1791.
(17) Sato, O.; Cui, A.; Matsuda, R.; Tao, J.; Hayami, S. *Acc. Chem. Res.* **2007**, *40*(5), 361–369.
(18) Beni, A.; Dei, A.; Laschi, S.; Rizzitano, M.; Sorace, L. *Chem.—Eur. J.* **2008**, *14*(6), 1804–1813.
(19) Beni, A.; Dei, A.; Rizzitano, M.; Sorace, L. *Chem. Commun.* **2007**, 2160–2162.
(20) Carbonera, C.; Dei, A.; Létard, J.-F.; Sangregorio, C.; Sorace, L. *Inorg. Chim. Acta* **2007**, *360*(13), 3825–3828.

 Published on Web 02/23/2010

Table 1. Crystallographic Data and Refinement Parameters for **1**

	ls-Co^{III}(Cat)(SQ)(4-CNpy)$_2$	*hs*-Co^{II}(SQ)(SQ)(4-CNpy)$_2$
chemical formula	$C_{40}H_{48}CoN_4O_4$	$C_{40}H_{48}CoN_4O_4$
M (g·mol^{-1})	707.75	707.75
crystal system, space group	monoclinic, $P2_1/c$	monoclinic, $P2_1/c$
a (Å)	11.6531(8)	11.7031(5)
b (Å)	22.4266(14)	22.8781(9)
c (Å)	7.2851(5)	7.2110(3)
α (deg)	90.00	90.00
β (deg)	91.665(4)	90.209(3)
γ (deg)	90.00	90.00
V (Å^3)	1903.1(2)	1930.69(14)
ρ (g/cm^3)	1.235	1.217
Z	2	2
T (K)	95	143
μ, (cm^{-1})	0.495	0.488
refinement method	full matrix least-squares using F^2	full matrix least-squares using F^2
final R indices [$I > 2\sigma(I)$][a]	R_1 = 0.0802 wR2 = 0.1891	R_1 = 0.0664 wR2 = 0.1775
R indices (all data)[a]	R_1 = 0.1375 wR2 = 0.2137	R_1 = 0. 1004 wR2 = 0.1973
GOF	1.080	1.167

[a] $R1 = \sum||F_o| - |F_c||/\sum|F_o|$; $wR2 = [\sum w(F_o^2 - F_c^2)^2/\sum w(F_o^4)]^{1/2}$.

studying this phenomenon. We present herein a valence tautomeric cobalt complex of a classic topology,[21] where the mixed-valent dyad of the Co^{III} form is composed of 3,5-di-*t*-butyl-SQ and -Cat and the remaining coordination sites are occupied by 4-cyanopyridine (4-CNpy): Co^{III}(SQ)(Cat)-(4-CNpy)$_2$ (**1**). The magnetic behavior of this complex in response to both thermal- and photochemical stimuli is very interesting, and bears more similarity to classical LIESST complexes, than photoinduced valence tautomeric complexes.[7,8,17]

Experimental Section

General Considerations. Elemental Analyses (C, H, and N) were performed by Atlantic Microlab, Inc., Norcross, GA. Infrared spectra were collected on a Perkin-Elmer Spectrum RX-1 FT-IR Spectrometer for samples cast as a film from CH_2Cl_2 on a NaCl plate. Unless noted otherwise, all reactions were performed in oven-dried glassware under a nitrogen atmosphere. Toluene was collected from an alumina column solvent purification system.[22] $[Co(SQ)_2]_4$ was prepared according to published methods.[23] 4-Cyanopyridine was used as received, without further purification. SQ = 3,5-di-*t*-butyl-*o*-semiquinonate, Cat = 3,5-di-*t*-butyl-*o*-catechol.

Preparation of Co^{III}(SQ)(Cat)(4-CNpy)$_2$, 1:[12]. To a 250 mL oven-dried Schlenk flask is added $[Co^{II}(SQ)_2]_4$ (226 mg, 0.11 mmol) and 70 mL of toluene, affording a green solution. To this mixture is added 4-cyanopyridine (95 mg, 0.91 mmol) as a solution in 20 mL of toluene. The reaction mixture is stirred, shielded from light, and heated to 35 °C for 5 h. Concentration of the dark blue mixture affords **1** as blue needles (220 mg, 69%). IR (film from CH_2Cl_2) ν in cm^{-1}: 6773(b), 4760(b), 3072, 2949, 2916, 2874, 2235, 1715, 1665, 1579, 1462, 1412, 1361, 1287, 1246, 1206, 1095, 1065, 1025, 984, 902, 860, 829, 784, 738, 656. Anal. Calcd $C_{40}H_{48}CoN_4O_4$; C, 67.88; H, 6.84; N, 7.92. Found C, 67.91; H, 6.73; N, 7.70.

Magnetometry. Magnetic susceptibilities were measured on a Quantum Design MPMS-XL7 SQUID Magnetometer using an applied field of 0.7 T for Curie plots. Microcrystalline samples (ca. 5 mg) were loaded into gelcap/straw sample holders and mounted to the sample rod with Kapton tape. Data from the gelcap samples were corrected for the sample container and molecular diamagnetism using Pascal's constants[24] as a first approximation. The data was further corrected for inaccuracies in the diamagnetic correction by incorporation of a straight line, the slope of which represents the residual diamagnetic correction.

Photochemical Experiments. Magnetic susceptibilities were measured on a Quantum Design MPMS-XL7 SQUID Magnetometer with an applied field of 0.7 T for Curie plots. Crystalline samples (< 1.0 mg) were loaded into a quartz cup and placed into a Fiberglide Industries fiber optic rod assembly for photoexcitation experiments. The samples were photolyzed with a Dolan-Jenner Fiber-Lite Model 180 high intensity fiber optic illuminator, equipped with a tungsten-halogen EKE lamp (150 W, λ = 400 nm−850 nm). The data for the fiber optic samples were corrected for the inherent diamagnetism of the sample holder through a background scan subtraction and for molecular diamagnetism through Pascal's constants.[24]

X-ray Crystallography. All X-ray measurements were made on a Bruker-Nonius Kappa Axis X8 Apex2 diffractometer on samples mounted on a nylon loop with a small amount of Paratone N oil. The sample was introduced to the diffractometer at 125 K before being cooled at a rate of 6 K/min to 95 K for data collection. Following the initial collection, the sample was warmed from 95 to 293 K at a rate of 6 K/min and left at that temperature for 20 min to melt the accumulated ice and blow off any residual moisture. The sample was then cooled to 143 K at a rate of 6 K/min for data collection. Crystallographic data and refinement details are summarized in Table 1.

Results and Discussion

The structural features of this complex are heavily dependent on the electron distribution within the system (i.e., *ls*-Co^{III}(Cat)(SQ) vs *hs*-Co^{II}(SQ)(SQ)). As such, an initial discussion of the magnetic behavior is necessary, to establish the temperature stability ranges of each tautomeric form and highlight the dependence of the magnetic behavior on the solid state structure. This allows for a judicious selection of temperatures for X-ray data collection to ensure pure structures of the *ls*-Co^{III} and *hs*-Co^{II} forms for comparison.

Variable Temperature Magnetic Susceptibility. The variable temperature paramagnetic susceptibility (χ_{para})

(21) Attia, A. S.; Junga, O.-S.; Pierpont, C. G. *Inorg. Chim. Acta* **1994**, *226* (1−2), 91–98.
(22) Pangborn, A. B.; Giardello, M. A.; Grubbs, R. H.; Rosen, R. K.; Timmers, F. J. *Organometallics* **1996**, *15*(5), 1518–1520.
(23) Buchanan, R. M.; Fitzgerald, B. J.; Pierpont, C. G. *Inorg. Chem.* **1979**, *18*(12), 3439–3444.
(24) Kahn, O. *Molecular Magnetism*; VCH Publishers, Inc.: New York, 1993; p 380.

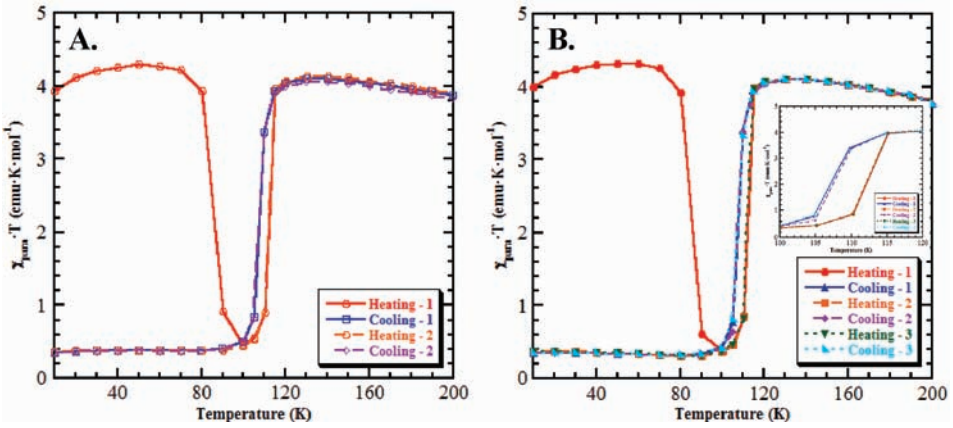

Figure 1. Variable-temperature magnetic susceptibility (χ_{para}) cycles of **1** plotted as $\chi_{para} \cdot T$ vs T accompanied by hysteresis (ca. 5 K). (A) First heating curve demonstrating thermal trapping of high temperature stable form upon rapid quench from 300 to 10 K, with thermal erasure at about 90 K.[25] (B) Additional cycles demonstrating independence of decay and hysteresis loops on thermal scanning rate.[26].

data for **1** are presented in Figure 1A as the paramagnetic susceptibility temperature product, $\chi_{para} \cdot T$, for two complete thermal cycles, and requires some comment. The high and low temperature stable forms of this complex are expected to be *hs*-Co^{II}(SQ)(SQ)(4-CNpy)$_2$ and *ls*-Co^{III}-(Cat)(SQ)(4-CNpy)$_2$, respectively. The former possesses a larger value of $\chi_{para} \cdot T$, because of the two $S = 1/2$ SQ ligands, and a single *hs*-Co^{II} $S = 3/2$ center, compared to the single $S = 1/2$ SQ of the latter. However, the initial heating curve after quenching the sample (300 K → 10 K in ca. 5 s) demonstrates a value of $\chi_{para} \cdot T$ at 10 K consistent with the high temperature form, which persists until about 90 K (T_{decay}). This behavior is absent in the subsequent cooling curve and the second thermal cycle, indicative of thermally trapping the high temperature form by rapid quenching. This feature can be eliminated by introducing the sample to the SQUID cavity at a temperature above the decay temperature and slowly cooling to 10 K at a rate of 10 K/min before experimentation. The initial observation of the decay of this spin state trapping feature occurred with a thermal scan rate of 3 K/min; no change was observed in the behavior upon reducing the scan rate to 1 K/min (Figure 1B). The heating and cooling cycles are also accompanied by a thermal hysteresis loop of about 5 K, centered about a $T_{1/2}$ value of 110 K (scan rate 105 K−120 K of 2 K/min). Subsequent experiments with varying thermal scanning rates (105 K−120 at 1 K/min and 5 K/min) reveal that the hysteresis loop is indeed independent of scanning rate (Figure 1B, inset).

X-ray Crystallography. Schematic structures of **1** are presented in Figure 2, along with ORTEP drawings of the crystal structure. As the complex demonstrates a sharp conversion centered about 110 K (Figure 1), X-ray structures were collected on a single crystal at either side of the transition temperature, 95 and 143 K, to obtain crystallographic details of both tautomeric forms. The data in Table 1 describe the crystallographic parameters for the two tautomeric forms, presenting identical space groups but rather dramatic and anisotropic changes to the unit cell parameters. A slight expansion along ***a*** (0.4%) is observed. More dramatic is the 1% contraction along ***c*** and the 2% (0.4 Å) expansion of the ***b*** lattice constant. This shows that the molecular geometry does not demonstrate stark changes across the valence tautomeric transition; however, there is definite expansion of the coordination sphere by approximately 0.15 Å, as is observed in other *ls*-Co^{III}(SQ)(Cat)L ↔ *hs*-Co^{II}(SQ)-(SQ)L valence tautomeric systems.[12,13,27] A simple expansion of the coordination sphere does not account for the anisotropic nature of the unit cell expansion. Instead this points toward a significant molecular reorientation within the ***b-c*** plane associated with the phase transition.

The coordination sphere expansion of about 0.15 Å accompanying conversion from Co^{III} → Co^{II} derives from the Co-L bond length expansion, because of both the increase in ionic radius of Co^{II} and the population of dσ* metal orbitals.[28] Also, in the *ls*-Co^{III}(SQ)(Cat)L ↔ *hs*-Co^{II}(SQ)(SQ)L conversion the dioxolene (diox) valence changes, where the decrease in C−O bond lengths from Cat → SQ (because of depopulation of π*-type orbitals) is well characterized.[13,27] Table 2 summarizes the relevant bond lengths for both tautomeric forms of **1**. In the structures of **1**, the cobalt sits on a crystallographically imposed inversion center, coincident with the molecular C_2 axis, resulting in averaged bond distances. As such, X-ray crystallography cannot distinguish between averaged bond lengths due to positional disorder and mixed-valent (Cat/SQ) delocalization; inspection of these bond lengths can merely confirm the $[Co^{III}(diox)_2]^0$ or $[Co^{II}(diox)_2]^0$ oxidation state.

The marked deviation in the Co−N bond length (Table 2) relative to the Co−O bonds appears to be of significance, as it presents the largest change within the coordination sphere. This suggests that the motion of the pyridine plays a major role in the tautomerization event.

(25) Heating and Cooling rates: 10 K−100 K range, 3 K/min; 105 K−120 K range, 2 K/min; 130 K−300 K range, 5 K/min.

(26) Scan 1 - Heating rates: 10 K−100 K range, 1 K/min; 105 K−120 K range, 2 K/min; 130 K−300 K range, 5 K/min, Cooling rates: 10 K−100 K range, 3 K/min; 105 K−120 K range, 2 K/min; 130 K−300 K range, 5 K/min; Scan 2 - Heating and Cooling rates: 10 K−100 K range, 3 K/min; 105 K−120 K range, 1 K/min; 130 K−300 K range, 5 K/min; Scan 3 - Heating and Cooling rates: 10 K−100 K range, 3 K/min; 105 K−120 K range, 5 K/min; 130 K−300 K range, 5 K/min.

(27) Adams, D. M.; Noodleman, L.; Hendrickson, D. N. *Inorg. Chem.* **1997**, *36*(18), 3966–3984.

(28) *CRC Handbook of Chemistry and Physics*. 88th ed.; CRC Press, Taylor & Francis Group: New York, 2008.

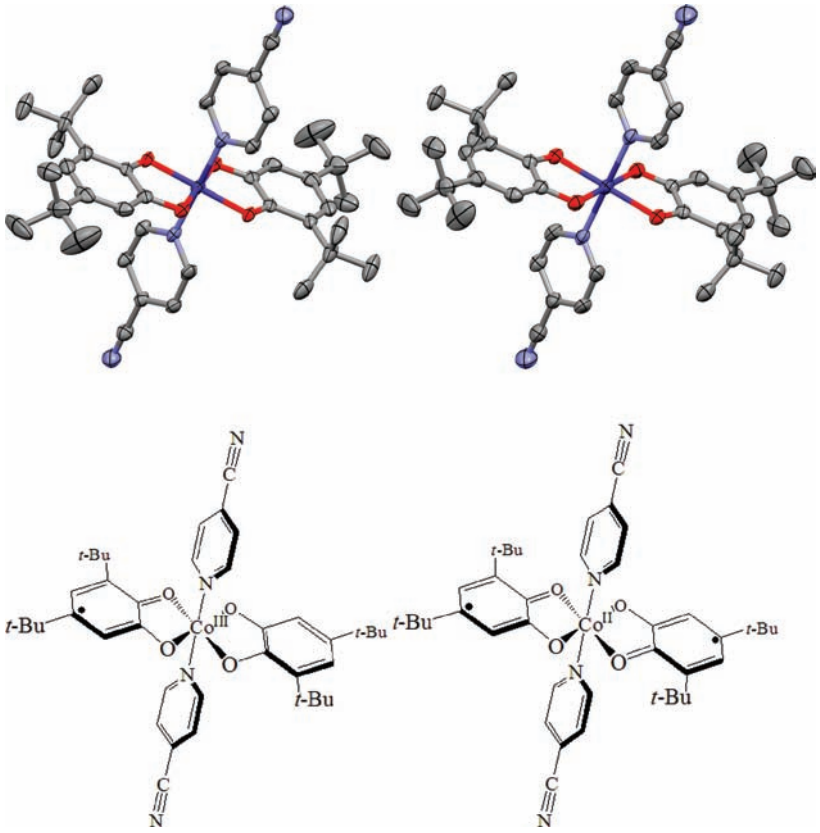

Figure 2. Structure of **1**, using 50% thermal ellipsoids. Hydrogen atoms have been omitted for clarity. (Top) ORTEP structures of *ls*-Co^{III}(Cat)(SQ)(4-CNpy)$_2$ (Left) and *hs*-Co^{II}(SQ)(SQ)(4-CNpy)$_2$ (Right), (Bottom) Bond-line drawings of *ls*-Co^{III}(Cat)(SQ)(4-CNpy)$_2$ (Left) and *hs*-Co^{II}(SQ)(SQ)(4-CNpy)$_2$ (Right).

Table 2. Selected Bond Distances for Co^{III}(Cat)(SQ)(4-CNpy)$_2$, **1**, with Literature Comparison

	1, $Co^{III}(diox)_2$ 95 K	**1**, $Co^{II}(diox)_2$ 143 K	Δ, (Co^{II}−Co^{III})	$Co^{III}(diox)_2(phen)^a$ 173 K	$Co^{II}(diox)_2(phen)^a$ 295 K	Δ, (Co^{II}−Co^{III})
Co−O_1 (Å)	1.888(3)	2.014(2)	0.126	1.891(8)^b	2.049(9)^b	0.158
Co−O_2 (Å)	1.894(3)	2.029(2)	0.135	1.890(8)^b	2.057(10)^b	0.167
Co−N_1 (Å)	1.964(4)	2.161(3)	0.197	1.932(10)^b	2.137(15)^b	0.205
C_1−O_1 (Å)	1.325(5)	1.298(4)	−0.027	1.329(16)^b	1.279(18)^b	−0.05
C_2−O_2 (Å)	1.320(5)	1.291(4)	−0.029	1.312(16)^b	1.283(10)^b	−0.029
a (Å)	11.6531(8)	11.7031(5)	0.0500	10.391(6)	10.436(4)	0.045
b (Å)	22.4266(14)	22.8781(9)	0.4515	31.692(17)	32.524(14)	0.832
c (Å)	7.2851(5)	7.2110(3)	−0.0741	13.164(7)	13.563(6)	0.399

[a] Taken from reference 13, phen = phenanthroline. [b] Averaged values.

Interesting too is that in **1** the Co−N bonds effectively lie within the crystallographic ***b-c*** plane; the plane that exhibits the greatest lattice variation across the phase transition. Inspection of the intermolecular contacts within the crystal lattice of **1** (Figure 3) reveals several important intermolecular interactions. Close contacts are observed between the terminal nitrogen (N(2)) of one cyanopyridine and a hydrogen (H(16)) *ortho*- to the cyano- of a 4-cyanopyridine neighbor related by the ***c***-glide.[29,30] An additional set of close contacts exists between the other hydrogen *ortho*- to the cyano- and the O(1) of the diox ligand neighbor related by translation along ***c***. These contacts, N(2)--H(16) = 2.45 Å and O(1)--H(18) = 2.30 Å in the *ls*-Co^{III} structure and N(2)--H(16) = 2.48 Å and O(1)--H(18) = 2.30 Å in the *hs*-Co^{II} structure, are well within the sum of the van der Waals radii (N = 1.55 Å, O = 1.52 and H = 1.20 Å)[31] indicative of (1) a C−H···N hydrogen bonding interaction involving the cyano-nitrogen and (2) a C−H···O interaction involving the diox-oxygen, to the edge of the adjacent pyridine.[29−32] Together the pairwise donor/acceptor linkages of the cyanopyridine ligands staggered across the ***c***-glide and the diox/cyanopyridine ligands translated along ***c*** create a reasonably strong hydrogen-bonded molecular chain. The *trans*-coordination of cyanopyridine ligands to cobalt results in these chains being strongly linked along the ***b*** direction as well, forming a strong two-dimensional lattice in the ***b-c*** plane. Interestingly, the cyano → pyridine and diox → pyridine hydrogen-bond contacts do not significantly change between the structures of the high-spin

(29) Marjo, C.; Bishop, R.; Craig, D. C.; Scudder, M. L. *Eur. J. Org. Chem.* **2001**, *2001*(5), 863–873.
(30) Rahman, A. N. M. M.; Bishop, R.; Craig, D. C.; Scudder, M. L. *Eur. J. Org. Chem.* **2003**, *2003*(1), 72–81.
(31) Bondi, A. *J. Phys. Chem.* **1964**, *68*(3), 441–451.
(32) Desiraju, G. R.; Steiner, T. *The Weak Hydrogen Bond in Structural Chemistry and Biology*; Oxford University Press: New York, 1999.

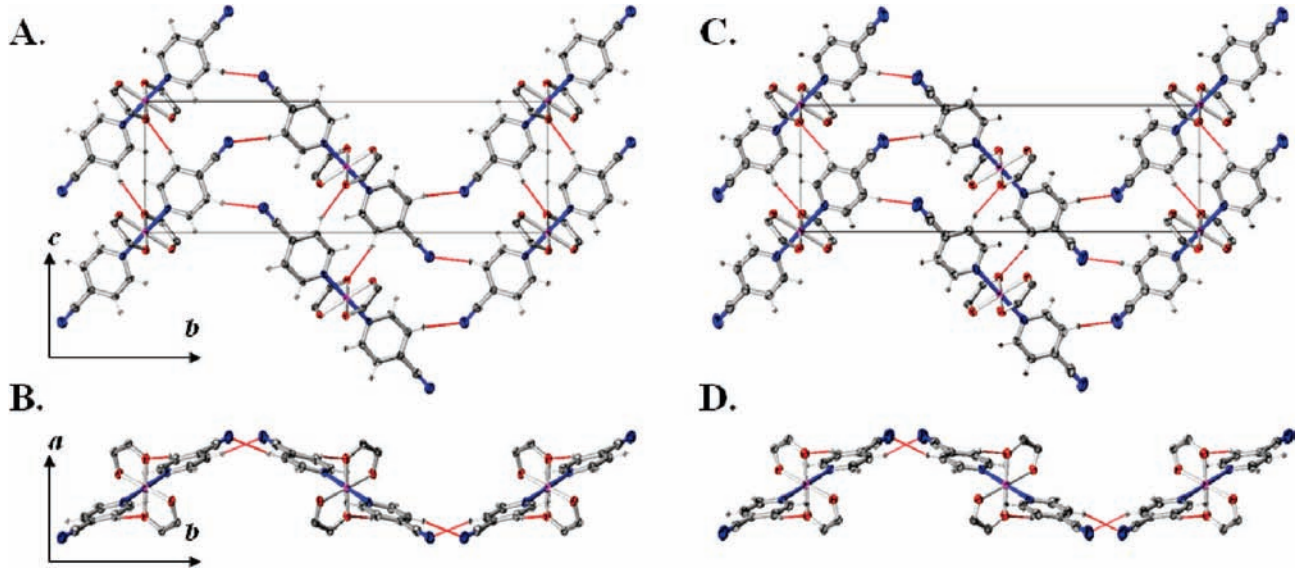

Figure 3. Crystal packing diagrams of **1** in the *ls*-Co^{III} (Left) and *hs*-Co^{II} (Right) forms. Views A and C are the respective structures viewed down the *a*-axis; views B and D are viewed down the *c*-axis. Relevant H-bonding interactions are represented as red contacts.

and low-spin tautomers in spite of the relatively large change in the Co−N and Co−O distances, ~0.2 Å and ~0.1 Å, respectively. To accommodate the expansion in the local molecular coordination while retaining a constant intermolecular hydrogen-bonded lattice, the molecules must rotate within the ***b-c*** plane resulting in the anisotropic contraction along ***c*** and expansion along ***b***. Furthermore, that the hydrogen-bond distances change very little between the two tautomers speaks to the role of this hydrogen-bonded lattice in stabilizing both forms. This hydrogen bonding can act to provide a mechanism to facilitate the *ls*-Co^{III} → *hs*-Co^{II} conversion, by lowering the activation barrier for Co−N and Co−O bond length elongation. The hydrogen-bonded lattice can similarly stabilize the expanded *hs*-Co^{II} tautomer. Together these lattice effects may account for the observed hysteresis of the valence tautomeric transiton.

Photoinduced Valence Tautomerism. The ability to thermally trap the high-temperature stable Co^{II} form of this complex by rapid quenching suggests metastability at low temperatures. The common tool used to probe both accessibility and stability of the metastable Co^{II} form is irradiation with a SQUID-mounted laser source.[1,4,7,8,17,19] Lacking access to such a laser, the metastability of **1** was tested at 10 K by irradiation with a white light source (150 W, λ = 400−850 nm). Previously reported complexes of this type demonstrating photoinduced activity often reach photostationary limits, after reaching conversion percentages ranging from 5−30%.[15,19,20] In our experience the photostationary limit of **1** at 10 K was never reached, even after 12 h of irradiation, with conversion percentages approaching 30%.[33] Moreover, the metastable state is readily accessible under irradiation at temperatures approaching 80 K. Figure 4 illustrates two thermal cycles following irradiation at 10 K, where the light source was removed for the thermal scans. The

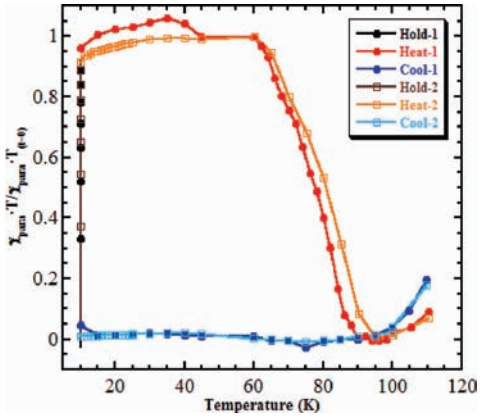

Figure 4. . Photogeneration/thermal decay cycles of the *hs*-Co^{II}-form of **1** from 10 K−110 K (2 K/min rate).[34].

stability from 10−70 K is virtually identical to the behavior of the thermally quenched fraction, with rapid thermal decay at about 90 K. This suggests that the photogenerated form and the thermally trapped form are indeed the same species. The photogeneration/thermal decay cycle can be repeated many times on the same sample without any appreciable decrease in the maximum value of $\chi_{para} \cdot T$.

***hs*-Co^{II} → *ls*-Co^{III} Relaxation.** This remarkable behavior observed for **1** strongly resembles the LIESST-based behavior in iron spin crossover complexes.[1,2,4,5,7−10] The plateau in $\chi_{para} \cdot T$ from about 10 K−70 K is reminiscent of the behavior and stability observed in these iron systems,[5,7−10] and is in stark contrast to the behavior observed for the more closely related photoinduced valence tautomeric systems.[15,17,19,20,35−37] To compare the kinetic stability of the photogenerated form of **1** to that of

(33) This threshold is likely due to irradiation of both Co^{III} and Co^{II} bands reaching a steady state of photoexcitation/photodecay.

(34) The data from 45 K−55 K are obscured because of a phase transition in oxygen trapped in the sample cavity and has been omitted.

(35) Beni, A.; Carbonera, C.; Dei, A.; Létard, J.-F.; Righini, R.; Sangregorio, C.; Sorace, L. *J. Braz. Chem. Soc.* **2006**, *17*(8), 1522.

(36) Beni, A.; Dei, A.; Shultz, D. A.; Sorace, L. *Chem. Phys. Lett.* **2006**, *428*(4−6), 400–404.

(37) Carbonera, C.; Dei, A.; Sangregorio, C.; Létard, J.-F. *Chem. Phys. Lett.* **2004**, *396*(1−3), 198–201.

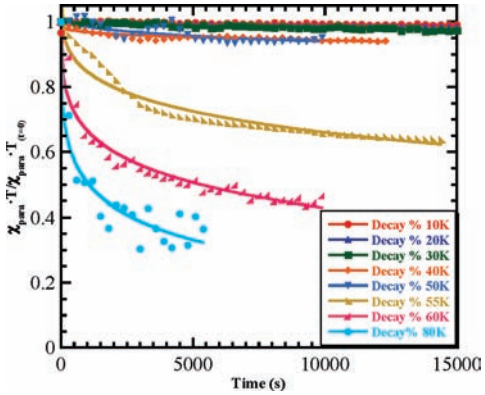

Figure 5. Decay kinetics following irradiation at 10 K. The lines represent the best fit to the stretched exponential described in the text.

Table 3. Summary of Estimated Lower Limit Lifetimes with Literature Values

temperature (K)	stretched exponential fit: lit. τ (s)[19,38]	lower limit: $Co^{III}(SQ)(Cat)(4\text{-}CNpy)_2$, **1**, τ (s)[a]	lower limit: lit. τ (s)[19,38]
10	2.0×10^{6b}	1.6×10^{6}	3.5×10^{5b}
	8.2×10^{6c}		2.9×10^{5c}
20	4.0×10^{6b}	1.2×10^{6}	1.9×10^{5b}
	2.2×10^{6c}		1.6×10^{5c}
30	9.1×10^{5b}	5.8×10^{5}	1.3×10^{5b}
40	3.6×10^{5b}	2.0×10^{5}	9.2×10^{4b}
	1.7×10^{5c}		5.6×10^{4c}
50	1.1×10^{5b}	1.3×10^{5}	5.0×10^{4b}
	4.9×10^{4c}		2.7×10^{4c}
60	6.3×10^{4b}	1.2×10^{4}	3.7×10^{4b}
70	2.3×10^{4b}		2.2×10^{4b}
80		5.4×10^{3}	

[a] Near linear decay behavior suggesting indefinite stability and unreliable fits to a stretched exponential. [b] Taken from reference 38. [c] Taken from reference 19.

other valence tautomers, the lifetime, τ, at several temperatures was obtained from the decay of $\chi_{para} \cdot T$ (Figure 5, Table 3) following irradiation.[19,37,38] The rate constants are typically obtained from the best fit to a stretched exponential (eq 1), where $\chi_{para} \cdot T$ is the value at time t, $(\chi_{para} \cdot T)_{t=0}$ is the value at time $t = 0$, k is the rate constant ($\tau = 1/k$), and β is a parameter to compensate for a varying distribution of relaxation rates.[37] A value of $\beta = 0.3$ is most commonly used for similar systems.[36,37] Previously, the longest observed lifetime at 10 K of 8.2×10^6 s was reported for a $[Co^{III}(Metpa)(PhenCat)]PF_6$ complex,[19] presented in Table 3.

$$\frac{\chi_{para} \cdot T}{(\chi_{para} \cdot T)_{t=0}} = e^{(-kt)^{\beta}} \qquad (1)$$

Figure 5 depicts the observed decay kinetics, where a sample of **1** is irradiated at 10 K for about 10 h (ca. 30% conversion), heated to the desired temperature, and the value of $\chi_{para} \cdot T$ monitored over time following removal of the light source. At temperatures below about 50 K, there is no appreciable decay in the value of $\chi_{para} \cdot T$ after several hours, where temperatures of 60 K are required to approach 50% decay after about 3 h. The data below about 40 K behave as a near straight line (on the scale $0.0 < \chi_{para} \cdot T/(\chi_{para} \cdot T)_{t=0} < 1.05$), where at 30,000 s the value of $\chi_{para} \cdot T$ at 10 K decays by only 1.8%. This behavior is indicative of near indefinite stability of the photogenerated form at low temperatures. Fits of the kinetic decay traces to eq 1 afford lifetimes below about 40 K that are several orders of magnitude greater than those previously reported for $[Co^{III}(Metpa)(PhenCat)]PF_6$.[19,39] However, the exponential fits at these low temperatures provide unreliable lifetime values because of the high kinetic stability and near linear behavior on this time scale. From comparison of the decay trace of **1** at 10 K to those of $[\{Co(dpqa)\}_2(dhbq)](PF_6)_3$ and $[Co^{III}(Metpa)(PhenCat)]PF_6$ (see Supporting Information) it is clear that the lifetime of **1** far exceeds the reported values of 2.0×10^6 s and 8.2×10^6 s, respectively.[19,38,39] The curves appear to best match the 40 K trace of **1** (Supporting Information), where there is enough curvature to the decay curve to obtain a better fit, affording a lifetime about 2 orders of magnitude longer than $[Co^{III}(Metpa)(PhenCat)]PF_6$, and all previously reported lifetimes at 10 K.[17,19,38,39] In our analysis of the kinetic decay data we are thus faced with two choices: (1) report values consistent with the treatment of data in the literature by fitting to the stretched exponential,[19,37,38] affording unreasonably long values of τ for **1**,[39] with no physical significance because of the relatively short time scale of the experiment relative to τ, or (2) estimate a lower limit on the decay lifetimes for **1** and previously reported complexes[19,38] based on the final decay percentage and experimental time scale for comparison purposes. The results of the latter comparative analysis are presented in Table 3, along with the stretched exponential fit values from the literature.[19,38] The limiting values were calculated using eq 2 from the final decay percentage (estimated from literature data) and the time scale of the experiment.

$$\tau = -\frac{t}{\ln\left(\frac{\chi_{para} \cdot T}{(\chi_{para} \cdot T)_{t=0}}\right)} \qquad (2)$$

Comparison of the new lower limiting values of the lifetimes suggest that complex **1** demonstrates greater stability of at least an order of magnitude over these previously reported examples.

Conclusions

Valence tautomers of this structural type represent a new archetype in photoinduced valence tautomerism, demonstrating a highly stable photogenerated Co^{II} form, accessible also through rapid thermal quenching. The simplicity of the complex's molecular structure, ease of synthesis, and an abundance of readily available 4-substutited-pyridines favor this molecular architecture for intensive study of these effects. Irradiation with a broad spectrum white light source leads to high conversion percentages (ca. 30%) in comparison to monochromatic laser irradiation leading to conversions of

(38) Li, B.; Tao, J.; Sun, H.; Sato, O.; Huang, R.-B.; Zheng, L.-S. *Chem. Commun.* **2008**, *19*, 2269–2271.

(39) Lifetime from fit to stretched exponential (Eq. 1): 10 K−ca. 4×10^{10} s; 20 K−ca. 7×10^9 s; 30 K−ca. 9×10^8 s; 40 K−ca. 2×10^8 s; 50 K−ca. 3×10^7 s; 60 K−ca. 2×10^4 s; 80 K−4×10^3 s. See also Supporting Information, Figures 2 and 3.

5−30%. The kinetic stability of **1** is unmatched in the literature, with significant lifetimes at high (ca. 40 K) temperatures. The thermal stability of the photogenerated form of **1** represents the highest T_{decay} reported to date for photoinduced valence tautomerism. The mechanism for this enhanced stability appears to be rooted in the lattice stabilization caused by hydrogen bonding of the protons of the pyridine ligands with the cyano- substituent of a neighboring pyridine or one of the oxygens of neighboring diox ligands. A future report will summarize our investigations of an isostructural series to test the validity of the proposed mechanism of lattice-facilitated stability and thermal activity.

Acknowledgment. D.A.S. thanks the National Science Foundation (CHE-0345263/0910585) for financial support. The authors wish to acknowledge Dr. Paul D. Boyle of North Carolina State University for X-ray crystallographic data collection and refinement. The authors would like to thank reviewer no. 1 for his/her insightful comments.

Supporting Information Available: Crystallographic details for **1** (CIF), saturation magnetization, kinetic decay comparisons. This material is available free of charge via the Internet at http://pubs.acs.org.